Multichannel scattering mechanism behind the reentrant conductance feature in nanowires subject to strong spin-orbit coupling

Iann Cunha,[1] Leonardo Villegas-Lelovsky,[1,2] Victor Lopez-Richard,[1] and Leonardo Kleber Castelano[1,*]
[1]*Departamento de Física, Universidade Federal de São Carlos, 13565-905 São Carlos, São Paulo, Brazil*
[2]*Departamento de Física, IGCE, Universidade Estadual Paulista, 13506-900 Rio Claro, São Paulo, Brazil*

(Received 17 February 2020; revised 14 October 2020; accepted 5 November 2020; published 18 November 2020)

The characterization of helical states can be performed by checking the existence of the reentrant behavior, which appears as a dip in the conductance probed in nanowires (NWs) with strong spin-orbit coupling (SOC) and under a perpendicular magnetic field. Yet puzzling experimental results report the observation of the re-entrant behavior also in the absence of magnetic fields, ascribed to unconventional spin-flipping two-particle backscattering. We theoretically demonstrate that the observation of the conductance dip can be explained through a multichannel scattering mechanism, which causes a reduction of the transmission when an effective attractive potential and coupling between different channels are present. Both ingredients are provided by the SOC in the transport properties of NWs. The relative effect of the sharpness of interfaces and external fields has also been assessed. The reduction of symmetry constraints of the NW is analyzed and proved to be important in the tuning of the reentrant characteristic.

DOI: 10.1103/PhysRevB.102.195423

I. INTRODUCTION

Topologically protected quantum computation can be achieved by employing Majorana zero modes [1]. Such Majorana states were predicted to be observed in nanowires (NWs) with strong spin-orbit coupling (SOC) in proximity to an *s*-wave superconductor and under the presence of an external magnetic field [2–4]. Semiconductor NWs based on InAs and InSb have a strong SOC and the experimental realization and characterization of such NWs have been recently explored to check the existence of helical states [5–8], which are closely related to Majorana zero modes. A signature to verify helical states is the so-called reentrant behavior [9], which appears as a measurable dip in the conductance when an external magnetic field is strictly different from zero. In Ref. [5], however, an unexpected result was observed: the appearance of the reentrant characteristic in the absence of the external magnetic field. This feature was attributed to spin-flipping two-particle backscattering [5,10,11]. Nonetheless, the dip at zero magnetic field may also appear in the presence of scattering by impurities [12,13]. Consequently, a clear explanation for the reentrant feature is still lacking, as stated in Ref. [8], and we also subscribe to that assertion.

In this paper, we want to shed light on the problem of the observation of the reentrant behavior when the magnetic field is absent by adding an essential ingredient that has clearly been previously overlooked. The preliminary theoretical prediction of a conductance dip was ascribed to the opening of a pseudogap in the energy dispersion of the NW by combining SOC and a magnetic field [9]. Both theoretical and experimental validations of such a prediction in InAs and InSb NWs have been attempted for some time [5–7,14–16]. However, the result found in Ref. [5] is surprising because no pseudogap is expected when the magnetic field is absent. In turn, theoretical models that predict the pseudogap opening require the concurrence of three factors: the SOC along the whole NW [9,15,16], a magnetic field, and a spatial potential localized in a finite region, which controls the reentrant behavior by tuning the energy into the pseudogap. Particularly, in the experiment described in Ref. [5], a perpendicular electric field is applied in a finite region along the longitudinal direction of the NW, as depicted in Fig. 1. Once an electric field is applied, the induced structural inversion asymmetry SOC emerges [17]. Also, the bias voltage applied between source and drain, as shown in Fig. 1, triggers a SOC. However, the electric field, E_x, applied between top and bottom gates is much higher, thereby causing a stronger SOC in the finite region of length L. In this paper we will unveil how this last external field configuration plays an important role in the transport properties and provide a clear explanation for the reentrant behavior in the absence of the magnetic field. To comprehend this effect, one needs to understand that the Rashba Hamiltonian limited to a finite region behaves as an attractive potential, as shown in Ref. [18]. Furthermore, it has been demonstrated that a resonant reflection (dip in the conductance) might occur if two conditions are satisfied: the scattering by an attractive potential and the coupling between different transport channels [19], even in the absence of a magnetic field. Precisely, these two ingredients are present in quasi-one-dimensional systems, such as NWs, where the SOC takes place in a finite region.

II. MODEL

We theoretically model the electronic transport through the nanowire where the Rashba SOC occurs in a region with length L along the z direction by the following Hamiltonian:

$$H = \left(\frac{p^2}{2m^*} + V_c(x, y)\right)\mathbf{I} + H_R, \tag{1}$$

*lkcastelano@ufscar.br

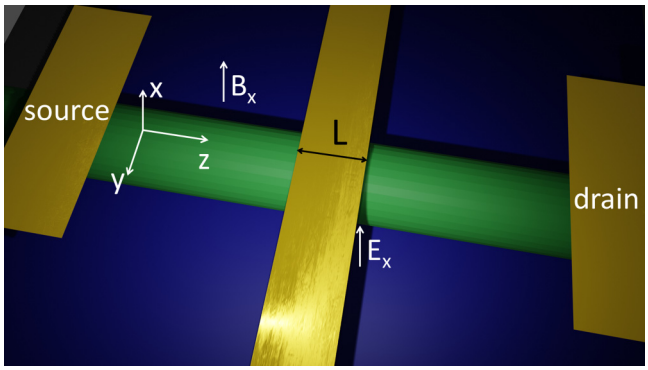

FIG. 1. Schematic picture showing the NW whose longitudinal direction coincides with the z axis. The source and the drain are presented along with the region with length L where the perpendicular electric field E_x between top and bottom gates is applied. The magnetic field, B_x, is applied in the x direction.

where the first term is the kinetic energy, $V_c(x, y)$ is the lateral confining potential, H_R is the Rashba Hamiltonian, and $\mathbf{I}$ is the 2×2 identity matrix corresponding to the spin-independent part. The confining potential describes the lateral confinement of the NW, which is modeled as $V_c(x, y) = m^*(\omega_x^2 x^2 + \omega_y^2 y^2)$, where ω_x and ω_y represent the strength of the lateral confinement in the x and y directions, respectively. We assume that the Rashba interaction, caused by the electric field E_x, acts only in the region of length L along the z direction; thus, $H_R = \alpha f(z)(k_y\sigma_z - k_z\sigma_y)$, where $f(z) = \Theta(z + L/2) - \Theta(z - L/2)$ and $\Theta(z)$ is the Heaviside function. The Rashba coupling constant is α, while k_q and σ_q are the wave vector and the Pauli spin matrix in the q direction, respectively.

The wave function $\Psi(\vec{r})$ can be expanded as a function of the lateral eigenfunctions $\phi_{n_x,n_y}(x, y)$, which are solutions of the two-dimensional harmonic oscillator with eigenenergies $\epsilon_{n_x,n_y} = \hbar\omega_x(n_x + 1/2) + \hbar\omega_y(n_y + 1/2)$, with $n_x = n_y = 0, 1, 2, \ldots$. The wave function has two spin components $\Psi^{\pm}(\vec{r}) = \sum_{n_x,n_y} \psi^{\pm}_{n_x,n_y}(z)\phi_{n_x,n_y}(\rho, \varphi)$, where $\psi^{s}_{n_x,n_y}(z)$ is the scattering wave function along the z axis for each transport channel $j = (n_x, n_y, s)$, and $s = \pm$. For this expansion, the matrix elements of Eq. (1) are

$$H_{j,j'} = \left[\frac{\hbar^2 k_z^2}{2m} + \epsilon_j\right]\delta_{j,j'} + c_{j,j'} + d_{j,j'}. \tag{2}$$

In Eq. (2), we have the spin degenerated orbital eigenenergy $\epsilon_j = \epsilon_{n_x,n_y}$, the intersubband term $c_{j,j'} = \alpha(z)\langle j|k_y\sigma_z|j'\rangle$, and the intrasubband term $d_{j,j'} = -\langle j|\{\alpha(z), k_z\}\sigma_y|j'\rangle$, where $\{\alpha(z), k_z\} = [\alpha(z)k_z + k_z\alpha(z)]/2$ and $\alpha(z) = \alpha f(z)$. These terms can be analytically calculated by means of the raising and lowering operators, whose results are $c_{j,j'} = -is\prime\delta_{s,s'}\frac{\alpha(z)}{\sqrt{2}l_y}[\sqrt{n'_y}\delta_{n_y,n'_y-1} - \sqrt{n'_y+1}\delta_{n_y,n'_y+1}]\delta_{n_x,n'_x}$, where $l_y = \sqrt{\hbar/(m^*\omega_y)}$ and $d_{j,j'} = -is\delta_{s,-s'}\{\alpha(z), k_z\}\delta_{n_x,n_x\prime}\delta_{n_y,n_y\prime}$. The intersubband term only couples states with different quantum number n_y, same spin, and same quantum number n_x; while the intrasubband term couples states with different spin and same quantum numbers n_x and n_y. Ideally, we should consider infinite transport channels (subbands) to completely solve the transport along the z direction, but the influence of high energy channels would exponentially decay if incoherent transport effects were considered, in the same way that occurs for the Shubnikov–de Haas oscillations [20]. Thus, to extract the basic physics of the dip in the conductance, we consider the coupling between the lowest energy states and $\omega_y \leqslant \omega_x$ (similar equations can be found for $\omega_y > \omega_x$). Within this subspace, we get the following Hamiltonian:

$$H = \begin{pmatrix} \frac{\hbar^2 k_z^2}{2m} + \epsilon_1 & i\{\alpha,\ k_z\} & -ir(z) & 0 \\ -i\{\alpha,\ k_z\} & \frac{\hbar^2 k_z^2}{2m} + \epsilon_2 & 0 & ir(z) \\ ir(z) & 0 & \frac{\hbar^2 k_z^2}{2m} + \epsilon_3 & i\{\alpha,\ k_z\} \\ 0 & -ir(z) & -i\{\alpha,\ k_z\} & \frac{\hbar^2 k_z^2}{2m} + \epsilon_4 \end{pmatrix}, \tag{3}$$

where $j = 1 \Rightarrow (0, 0, +)$, $j = 2 \Rightarrow (0, 0, -)$, $j = 3 \Rightarrow (0, 1, +)$, and $j = 4 \Rightarrow (0, 1, -)$. For these states, we have that $\epsilon_1 = \epsilon_2 = \epsilon = \hbar(\omega_x + \omega_y)/2$, $\epsilon_3 = \epsilon_4 = \lambda = \hbar(\omega_x + 3\omega_y)/2$, $r(z) = \alpha(z)/(l_y\sqrt{2})$, and the transport wave function can be written as $\Phi = (\psi^+_{0,0}(z)\ \psi^-_{0,0}(z)\ \psi^+_{0,1}(z)\ \psi^-_{0,1}(z))^t$. By using the linear combination between transport channels with same energy, $\chi^{\pm}_{n_x,n_y}(z) = (\psi^+_{n_x,n_y}(z) \pm i\psi^-_{n_x,n_y}(z))e^{\mp i\theta(z)}/\sqrt{2}$, where $\theta(z) = \int_0^z k_\alpha(z\prime)dz\prime$ and $k_\alpha(z) = m\alpha(z)/\hbar^2$, we rewrite the transport wave function in this new basis $\tilde{\Phi} = (\chi^+_{0,0}(z)\ \chi^-_{0,0}(z)\ \chi^+_{0,1}(z)\ \chi^-_{0,1}(z))^t$ and we arrive at the transformed Hamiltonian

$$H = \begin{pmatrix} \frac{-\hbar^2}{2m}\frac{d^2}{dz^2} + \epsilon + V_\alpha(z) & 0 & 0 & -ir(z)e^{-2i\theta(z)} \\ 0 & \frac{-\hbar^2}{2m}\frac{d^2}{dz^2} + \epsilon + V_\alpha(z) & -ir(z)e^{-2i\theta(z)} & 0 \\ 0 & +ir(z)e^{2i\theta(z)} & \frac{-\hbar^2}{2m}\frac{d^2}{dz^2} + \lambda + V_\alpha(z) & \\ +ir(z)e^{2i\theta(z)} & 0 & 0 & \frac{-\hbar^2}{2m}\frac{d^2}{dz^2} + \lambda + V_\alpha(z) \end{pmatrix}, \tag{4}$$

where the intrasubband term of the SOC contribution appears as an effective attractive quantum well potential $V_\alpha(z) = -\frac{m\alpha(z)^2}{2\hbar^2}$, as also described in Ref. [18]. Its width is determined by L and the depth by the Rashba coupling strength (proportional to the perpendicular electric field E_x). Equation (4) leads to equations coupled in pairs with the same spin in the σ_y basis, given by

$$\frac{-\hbar^2}{2m}\frac{d^2\chi^{\pm}_{0,0}(z)}{dz^2} + [\epsilon - E + V_\alpha(z)]\chi^{\pm}_{0,0}(z) - ir(z)e^{-2i\theta(z)}\chi^{\mp}_{0,1}(z) = 0, \tag{5}$$

$$\frac{-\hbar^2}{2m}\frac{d^2\chi^{\pm}_{0,1}(z)}{dz^2} + [\lambda - E + V_\alpha(z)]\chi^{\pm}_{0,1}(z) + ir(z)e^{2i\theta(z)}\chi^{\mp}_{0,0}(z) = 0 \tag{6}$$

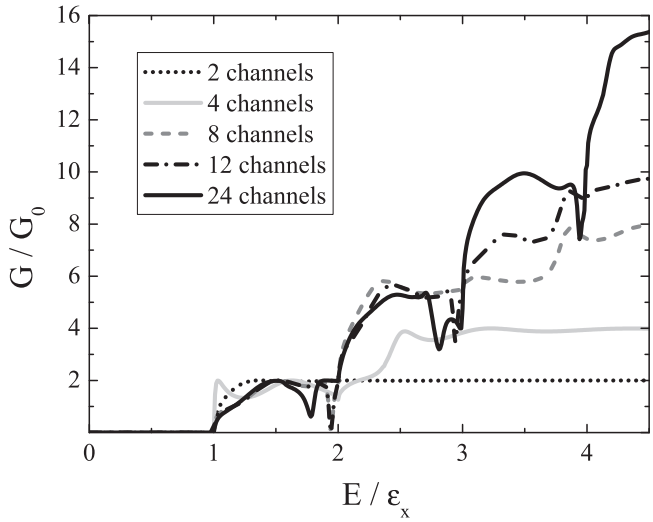

FIG. 2. Normalized conductance as a function of the normalized Fermi energy for 2, 4, 8, 12, and 24 channels, considering $L = 8.0l_x$, $\alpha = 1.0\alpha_0$, and null magnetic field.

Equations (5) and (6) were deduced in the simplest scenario to demonstrate that, by considering the coupling between only four states and the mere presence of the Rashba SOC within a finite region, the necessary conditions to observe the resonant reflection [19] are satisfied; they are (i) the existence of an attractive potential $V_\alpha(z)$ and (ii) the coupling between different channels ruled by the term $\pm ir(z)e^{\pm 2i\theta(z)}$. It is paramount to assert that a strict one-dimensional (1D) transport model, considering the Rashba SOC between different spins, will not lead to the required conditions described above because of the lack of the attractive potential. In Fig. 2, we plot the numerical solution for the normalized conductance as a function of the total energy, varying the number of states (channels) and considering $\alpha = \alpha_0$, $\omega_y = \omega_x$ and $L = 8.0l_x$, where $\varepsilon_x = \hbar\omega_x$, $l_x = \sqrt{\hbar/(m^*\omega_x)}$, and $\alpha_0 = \varepsilon_x l_x$, which are the chosen energy, length, and Rashba constant scales. The total energy, E, represents the applied bias, which in turn is equivalent to the variation of the gate-voltage applied perpendicularly to the NW [16]. The numerical results were obtained by noting that the total Hamiltonian in Eq. (1) commutes with the momentum in the z direction, p_z, therefore the scattering wave functions can be expanded in the $\exp(ik_z z)$ basis. By using the expansion of the wave-function in the $\exp(ik_z z)$ basis and the boundary conditions at the interfaces $z = \pm L/2$, we get a system of linear equations. The solution of this system of linear equations yields all the coefficients of the expansion in the $\exp(ik_z z)$ basis plus all the transmission and reflection coefficients [21]. The conductance is evaluated through the Landauer-Buttiker formula $G = G_0 \,\mathrm{Tr}\,[tt^\dagger]$, where $G_0 = e^2/h$ and t is the matrix composed of the transmission elements $t_{i,j}$, where i and j denote the transmitted and the incident channels, respectively.

III. RESULTS

In Fig. 2, the conductance is almost constant for $E > \varepsilon_x$ and no dip is observed if only two channels with quantum numbers $(0, 0, \pm)$ are taken into account (similarly to a strict 1D transport model). However, once four channels $\{(0, 0, \pm), (0, 1, \pm)\}$ are considered, a strong reflection occurs, leading to a dip in the conductance, as can be observed in the plot of normalized conductance shown in Fig. 2 for $E \approx 2\varepsilon_x$. The four-channels case corresponds to the numerical solution of Eqs. (5) and (6), which has the intrasubband Rashba SOC term equivalent to an attractive potential in the region $|z| \leqslant L/2$. Such a negative potential can support a quasibound state within this region and this state interacts with the continuum states causing the strong reflection due to interference effects. It is interesting to mention that, for $E < 2\varepsilon_x$, only the states $(0, 0, \pm)$ admit scattering modes, whereas the other quantum channels correspond to evanescent modes. Therefore, the influence of evanescent modes in the transport properties is very important, as can be seen when comparing the conductance evaluated using two and four channels in Fig. 2. Note that, in the isotropic case, with $\omega_y = \omega_x$, the states $(0, 1, \pm)$ and $(1, 0, \pm)$ are degenerated in energy, but only the state $(0, 1, \pm)$ couples to state $(0, 0, \pm)$; therefore, the conductance including the state $(1, 0, \pm)$ can be easily obtained by adding the constant value G_0 for $E > 2\varepsilon_x$ in the four-channels results of the conductance.

When eight channels are considered, $\{(0, i, \pm), (1, 0, \pm)\}$, with $i = 0, \ldots, 2$, the first dip moves to lower energies in the first plateau and no dip is observed for $E > 2\varepsilon_x$. The dip shifts because of the coupling between states $(0, 1, \pm)$ and $(0, 2, \pm)$, which affects the scattering mode $(0, 0, \pm)$. Again, degenerated states $(2, 0, \pm)$ and $(1, 1, \pm)$ do not couple to the scattering modes and only contribute with a constant value to the conductance evaluated with eight channels for $E > 3\varepsilon_x$. To facilitate the numerical calculations, degenerated states are not taken into account when they do not couple to the scattering modes within the total energy region considered, and their effect is only adding a constant value G_0 to the conductance when its channel is open.

Considering twelve channels, $\{(0, i, \pm), (1, j, \pm)\}$, with $i = 0, \ldots, 2$ and $j = 0, \ldots, 2$, the first dip does not change because the coupling with the scattering mode with quantum numbers $(0, 0, \pm)$ has not been modified. On the other hand, a dip in the second plateau appears for $E \approx 3\varepsilon_x$ due to the coupling between the scattering mode $(1, 0, \pm)$ and the evanescent modes $(1, 1, \pm)$ and $(1, 2, \pm)$. For 24 channels, $\{(0, i, \pm), (1, j, \pm), (2, k, \pm)\}$, with $i = 0, \ldots, 4$, $j = 0, \ldots, 3$, and $k = 0, \ldots, 2$, the first dip suffers a redshift due to the extra coupling between states $(0, 3, \pm)$ and $(0, 4, \pm)$. Two dips in the second plateau appear because of the inclusion of states $(0, 3, \pm)$, $(0, 4, \pm)$, and $(1, 3, \pm)$. Furthermore, a reentrance in the third plateau appears for $E \approx 4\varepsilon_x$ due to the coupling between states $(0, 2, \pm)$, $(0, 3, \pm)$, and $(0, 4, \pm)$. We can thus learn from the analysis of the results shown in Fig. 2 that for $E < \epsilon_{n_x,n_y}$ the scattering mode designated by quantum numbers (n_x, n_y, s) couples to the evanescent mode $(n_x, n_y + 1, s)$ through the intersubband term, which causes the dip in the conductance. On the other hand, evanescent modes $(n_x, n_y + 1, s)$ and $(n_x, n_y + 2, s)$ are coupled to each other, which modifies the conductance by a type of a domino effect. Of course, this domino effect keeps influencing the conductance up to a certain value of quantum numbers, where incoherent effects take place. Hereafter, the number of channels will be chosen depending on the range of energy studied

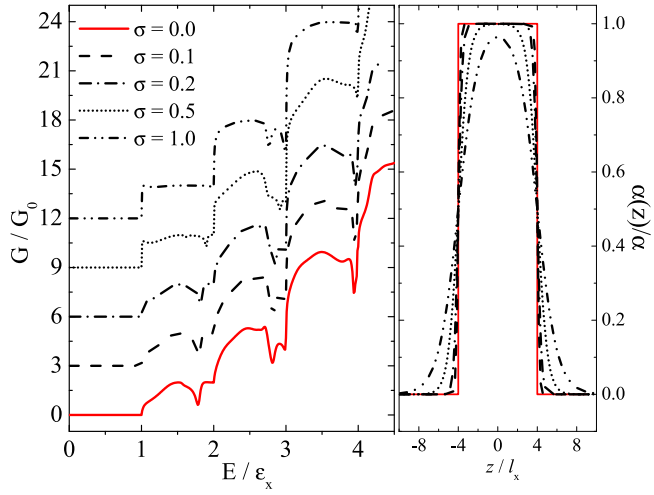

FIG. 3. (a) Normalized conductance as a function of the normalized Fermi energy for 24 channels, $L = 8.0l_x$, $\alpha = 1.0\alpha_0$, and null magnetic field, by changing the degree of smoothness of the SOC region, characterized by $\sigma = 0$ (solid curve), 0.1 (dashed curve), 0.2 (dash-dotted curve), 0.5 (dotted curve), and 1.0 (dash-do-dotted curve). (b) Spatial dependence of $\alpha(z)/\alpha$ for various values of σ.

and the ratio of $\omega_y = \omega_x$, but the minimum number of channels is fixed to 24.

According to Rainis and Loss [16], the smoothness of the electrostatic potential profile between the contacts and the wire plays an important role in the observation of the reentrant behavior for a finite magnetic field. They have shown that the electrostatic potential profile should not be either too smooth or too abrupt to optimize the observation of the dip in the conductance. Based on these discussions, we have also explored the effect of sharpness of the interfaces of the SOC region by adopting a spatial dependence of the Rashba coupling constant in the following way: $\alpha(x) = \alpha\{1/[1 + \exp((z - L/2)/\sigma)] - 1/[1 + \exp((z + L/2)/\sigma)]\}$, where σ is the degree of smoothness. As can be observed in Fig. 3, the conductance obtained in the abrupt case $\sigma = 0$ is not very different from the cases where $\sigma = 0.1$ and 0.2. Only for $\sigma = 0.5$ and 1.0 does the conductance become quantitatively different from the abrupt case, and the dip in the first plateau completely disappears when $\sigma = 1.0$. Therefore, we can conclude that the smoothness of the SOC region affects the dip of the conductance only when it is too smooth. Since the results of the sharp interfaces show a good agreement with the relatively smooth spatial dependence of the SOC region, we will hereafter employ the abrupt model in the numerical calculations.

The normalized conductance for different lengths of the SOC region is shown in Fig. 4(a), considering the following parameters: $L = 4.4l_x$ (solid curve), $L = 5.6l_x$ (dashed curve), $L = 6.8l_x$ (short-dashed curve), and $L = 8.0l_x$ (dotted curve), null magnetic field, $\omega_y = \omega_x$, and $\alpha = 1.0\alpha_0$. The dips can be tuned by modifying the length L [see Fig. 4(a)]. For example, the first dip disappears for $L = 5.6l_x$, while it reappears for $L = 4.4l_x$, $L = 6.8l_x$, and $L = 8.0l_x$. In the second plateau, one can find two dips ($L = 5.6l_x$, $L = 6.8l_x$, and $L = 8.0l_x$) or just one dip ($L = 4.4l_x$). In Fig. 4(b), we plot the normalized conductance for twenty four channels using the same

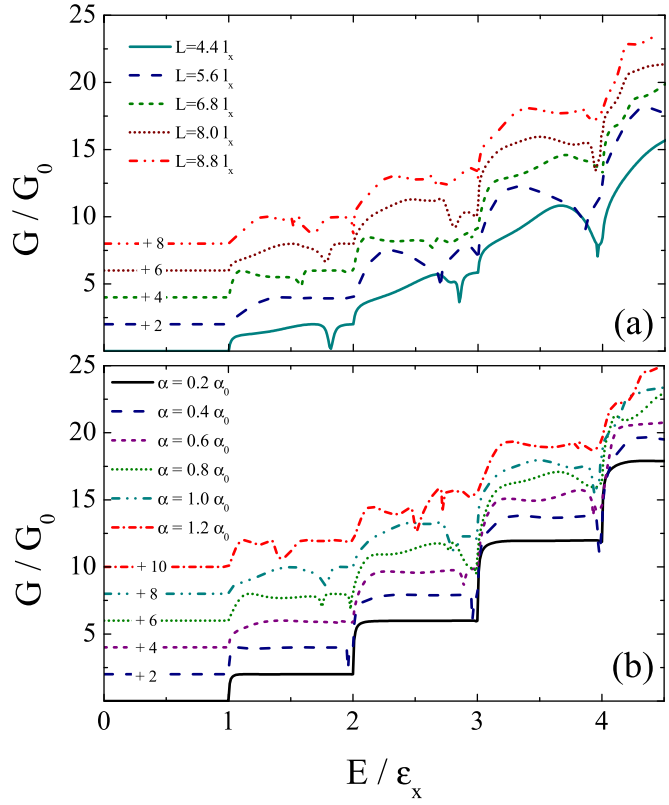

FIG. 4. (a) Normalized conductance as a function of the normalized Fermi energy for 24 channels, considering $L = 4.4l_x$, $5.6l_x$, $6.8l_x$, and $8.0l_x$, null magnetic field, and $\alpha = 1.0\alpha_0$. (b) Normalized conductance as a function of the normalized Fermi energy for 24 channels, considering $L = 8.0l_x$, null magnetic field, and $\alpha = 0.2\alpha_0$, $0.4\alpha_0$, $0.6\alpha_0$, $0.8\alpha_0$, $1.0\alpha_0$, and $1.2\alpha_0$. The curves are offset for clarity according to the indicated values.

parameters of Fig. 2, except for the Rashba constant, which is varied from $\alpha = 0.2\alpha_0$ to $\alpha = 1.2\alpha_0$. For $\alpha = 0.2\alpha_0$ no dips are observed in Fig. 4(b), but for $\alpha = 0.4\alpha_0$ the dips already appear. For $\alpha = 0.6\alpha_0$, the first dip disappears and the third dip gets wider. When $\alpha = 0.8\alpha_0$, two dips appear in the first plateau and the subsequent dips get wider. On the other hand, two dips appear in the second plateau and only one appears in the first plateau when $\alpha = \alpha_0$. For $\alpha = 1.2\alpha_0$, the dips in the first two plateaus suffer a redshift and the third dip almost disappears. In Ref. [5], the authors report two different values for the Rashba constant coupling $\alpha = 0.8$ eV Å and $\alpha = 1.2$ eV Å, which correspond to $\alpha = 0.57\alpha_0$ and $\alpha = 0.85\alpha_0$ in our simulations. These values are estimated from different experimental techniques and according to the results shown in Fig. 4(b), dips would appear for both experimental values. In summary, both parameters α or L induce the interference between scattering and evanescent modes, which can tune and lead to the appearance of the dips in the conductance.

In the experiment of Ref. [5], a conductance plateau around $G = 4G_0$ is observed, whereas in Figs. 2–4 the second plateau corresponds to $G = 6G_0$. This is caused by the symmetry of the lateral confinement that provides two scattering modes, $(0, 1, \pm)$ and $(1, 0, \pm)$, degenerated in energy. To obtain $G = 4G_0$, an asymmetry in the confinement of the NW that breaks this degeneracy must be considered. Thus, the cylindrical NW

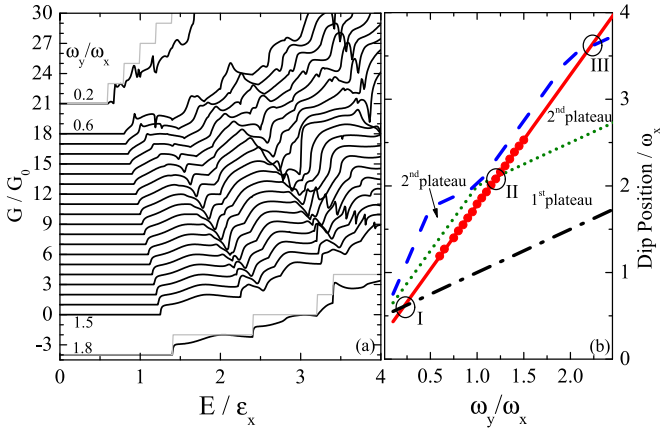

FIG. 5. (a) Normalized conductance as a function of the normalized Fermi energy for 24 channels, considering $L = 8.0l_x$, $\alpha = 1.0\alpha_0$, null magnetic field, and different values for $\gamma_{xy} = 0.2$, 0.6 to 1.5 (with step 0.05), and 1.8. The curves are offset for clarity. (b) The dotted points show the first dip position as a function of γ_{xy}. The red solid curve is the linear extrapolation of the first dip position. The black dash-dotted curve indicates the energy where the first step in the conductance appears. The green dotted curve shows where the transition between the first and second plateau occurs. The blue dashed curve shows where the transition between the second and third plateaus occurs.

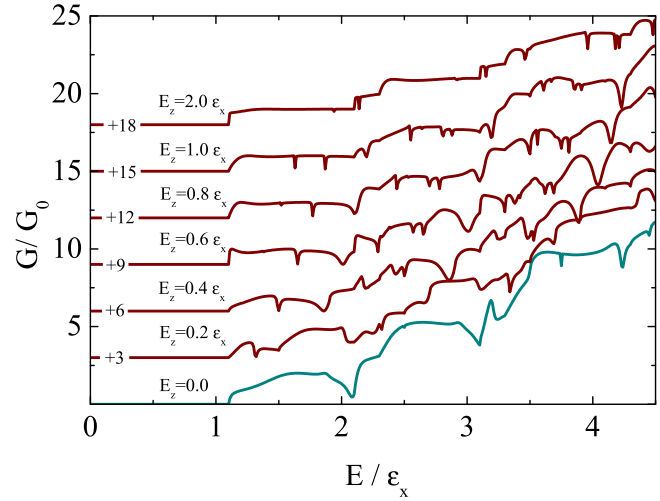

FIG. 6. Normalized conductance as a function of the normalized Fermi energy for 24 channels, considering $L = 8.0l_x$, $\alpha = 1.0\alpha_0$,$\omega_y = \omega_x$, and Zeeman energy in the range $E_Z = 0.0$–$2.0\varepsilon_x$. The curves are offset for clarity according to the indicated values.

can be replaced by an eccentric one, where the parameter $\gamma_{xy} = \omega_y/\omega_x = l_x^2/l_y^2$ represents the ratio between the square of the semiaxes of an ellipse in the x and the y directions. In Fig. 5(a), we plot the conductance considering different values of γ_{xy}. The gray (lighter) curves represent the conductance without SOC and they can be used as reference for the plateaus. For $\omega_y \neq \omega_x$, the conductance plateau around $G = 4G_0$ appears, as one can observe in Fig. 5(a) for null SOC (grey curves). In Fig. 5(b), we plot the first dip position (red dotted points) as a function of γ_{xy}. Moreover, the red solid curve is the linear extrapolation of the dip position. When $\gamma_{xy} = 0.2$, the first dip is absent [see Fig. 5(a)], and the reason for that can be understood by looking at the crossing [label I in Fig. 5(b)] between the extrapolated dip position and the black dash-dotted curve, which indicates the minimum energy required for nonzero conductance as a function of γ_{xy}. For $\gamma_{xy} \leqslant 0.2$, the dip does not occur because its position would be a nonallowed energy. This effect can also be explained due to the decreasing of the intrasubband term, which is proportional to $\alpha/\sqrt{l_y^2} = \sqrt{\gamma_{xy}}\hbar\omega_x\alpha/\alpha_0$. When $\gamma_{xy} \ll 1$, the intrasubband term becomes very small and the dips are suppressed. In other words, if the NW is very compressed in the x direction (same direction of E_x), the dips might completely vanish. In Fig. 5(b), the green dotted (blue dashed) curve shows the transition between the first (second) and second (third) plateau regions. When $\gamma_{xy} < 1.2$ the dip occurs within the first plateau region, which is delimited by the black dash-dotted curve and the green dotted curve in Fig. 5(b). When $1.2 \leqslant \gamma_{xy} \leqslant 2.2$ the dip occurs within the second plateau region, which is delimited by the green dotted curve and the blue dashed curve in Fig. 5(b). Qualitatively, the first dip position is pushed towards higher energies as a function of γ_{xy} and eventually the dip undergo transitions into higher plateaus as labeled as II and III in panel (b) of Fig. 5. Of course, there are other subtleties occurring as γ_{xy} is varied; for example, when $\gamma_{xy} = 0.7$ there is no dip in the first plateau. On the other hand, by increasing the value from $\gamma_{xy} = 0.75$ to $\gamma_{xy} = 1.5$ both the intensity and width of the first dip increase. Also, for $\gamma_{xy} = 0.6$ and 0.65 the first dip appears as well. All these subtleties occur due to interference phenomena. For $\gamma_{xy} = 1.8$, the dips in the first four plateaus are completely absent and this effect is related to the shift of the dip position to higher energies. Other dips position occurring in plateaus different than the first one shown in Fig. 5(a) also have a linear dependence on γ_{xy}, which is related to the subband energies that linearly vary as a function of γ_{xy}, thereby affecting the energy where the resonant reflection occurs.

In the experiment described in Ref. [5], it was also observed that the dip in the conductance appears for zero and for moderate values of the magnetic field, but disappears for high field values. To probe such effects in our theoretical model, we consider a uniform magnetic field applied in the x direction described by the Hamiltonian $H^Z = E_Z\sigma_x$, where E_Z is the Zeeman energy. The matrix elements for this Hamiltonian are given by $H^Z_{j,j'} = E_Z\delta_{n_x,n_{x'}}\delta_{n_y,n_{y'}}\delta_{s,-s'}$. Unlike the Rashba SOC, the magnetic field is present throughout the whole NW. When the magnetic field is included, the subband energy is shifted as $\epsilon_j^{\pm} = \epsilon_{n_x,n_y} \pm E_Z$. This would move the total energy where the first step in the conductance occurs. Yet, the electron source will be affected by the uniform magnetic field in the same way, thereby canceling out this energy shift. Thus, we have compensated for this difference and considered that the total energy where the first channel opens does not change with the variation of the magnetic field. In Fig. 6, we plot the normalized conductance for different values of the Zeeman energy, E_Z, as a function of the total energy. For $E_Z > 0$, the injection of only one electron occurs between $\epsilon_1 \leqslant E \leqslant \epsilon_1 + 2E_Z$, the injection of two electrons occurs after $E > \epsilon_1 + 2E_Z$, and so on. The range of energy between $E = 1.8\varepsilon_x$ and $E = 2.2\varepsilon_x$,

where the reduction of the conductance happens for $E_Z = 0$, still manifests in a similar way up to $E_Z = 0.8\varepsilon_x$. By using the experimental values for the g factor [5], we can estimate that $E_Z = 0.3\varepsilon_x$ would correspond to a magnetic field of 5 T. Furthermore, the increase of the magnetic field causes a narrowing of dips (see Fig. 6). We can thus ascribe the vanishing of the reentrant behavior for high magnetic fields observed in Ref. [5] to the combination of the dips' narrowing produced by increasing the magnetic field plus incoherent transport processes. The incoherent transport smears out the reentrant behavior [16] and for high values of the magnetic field it would not allow the appearance of very narrow regions of reflection.

IV. CONCLUSION

In conclusion, we presented a theoretical model capable of explaining the reentrant behavior of the conductance in the absence of the external magnetic field and that can be sustained also for finite field values. The dip in the conductance appears because of the resonant reflection which is predicted to occur in quasi-one-dimensional systems if two necessary conditions are met: the existence of an attractive potential and the coupling between different scattering channels, even though the coupling occurs between a scattering and an evanescent mode. Both conditions coexist when the NW experiences the Rashba SOC in a limited region of length L. The importance of the limited regions is related to the localized effective attractive potential that occurs when Rashba SOC is not extended but is locally present, enabling quasibound states that interfere with scattering modes, providing a suppression in the transmission. This scenario agrees with the experimental setup described in Ref. [5]. Furthermore, geometrical effects related to the symmetry of the horizontal cross section of the NW were explored and shown to be an important parameter to control the appearance and tuning of the dip in the conductance. Such geometrical effects can appear due to structural or external field configuration. Lastly, this work provides an alternative explanation to appearance of the reentrant characteristic for null magnetic field, which is simpler and more direct than the mechanism of spin-flipping two-particle backscattering [5,10,11], previously employed to address this phenomenon.

The data that support the findings of this study are available within the article.

ACKNOWLEDGMENTS

The authors are grateful for financial support by the Brazilian Agencies FAPESP, CNPq, and CAPES. L.K.C. acknowledges FAPESP (Grant No. 2019/09624-3) for supporting this research.

[1] C. Nayak, S. H. Simon, A. Stern, M. Freedman, and S. Das Sarma, Rev. Mod. Phys. **80**, 1083 (2008).
[2] J. Alicea, Y. Oreg, G. Refael, F. von Oppen, and M. P. A. Fisher, Nat. Phys. **7**, 412 (2011).
[3] Y. Oreg, G. Refael, and F. von Oppen, Phys. Rev. Lett. **105**, 177002 (2010).
[4] R. M. Lutchyn, J. D. Sau, and S. Das Sarma, Phys. Rev. Lett. **105**, 077001 (2010).
[5] S. Heedt, N. T. Ziani, F. Crepin, W. Prost, S. Trellenkamp, J. Schubert, D. Gruetzmacher, B. Trauzettel, and T. Schaepers, Nat. Phys. **13**, 563 (2017).
[6] J. Kammhuber, M. C. Cassidy, F. Pei, M. P. Nowak, A. Vuik, O. Gül, D. Car, S. R. Plissard, E. P. A. M. Bakkers, M. Wimmer, and L. P. Kouwenhoven, Nat. Commun. **8**, 478 (2017).
[7] I. van Weperen, S. R. Plissard, E. P. A. M. Bakkers, S. M. Frolov, and L. P. Kouwenhoven, Nano Lett. **13**, 387 (2013).
[8] J. Sun, R. S. Deacon, R. Wang, J. Yao, C. M. Lieber, and K. Ishibashi, Nano Lett. **18**, 6144 (2018).
[9] P. Středa and P. Šeba, Phys. Rev. Lett. **90**, 256601 (2003).
[10] C. J. Pedder, T. Meng, R. P. Tiwari, and T. L. Schmidt, Phys. Rev. B **94**, 245414 (2016).
[11] V. S. Khrapai and K. E. Nagaev, Phys. Rev. B **98**, 121401(R) (2018).
[12] J. C. E. Saldana, Y.-M. Niquet, J.-P. Cleuziou, E. J. H. Lee, D. Car, S. R. Plissard, E. P. A. M. Bakkers, and S. De Franceschi, Nano Lett. **18**, 2282 (2018).
[13] J. H. Bardarson, I. Magnusdottir, G. Gudmundsdottir, C.-S. Tang, A. Manolescu, and V. Gudmundsson, Phys. Rev. B **70**, 245308 (2004).
[14] Y. V. Pershin, J. A. Nesteroff, and V. Privman, Phys. Rev. B **69**, 121306(R) (2004).
[15] C.-S. Tang, Y.-H. Yu, N. R. Abdullah, and V. Gudmundsson, Phys. Lett. A **381**, 3960 (2017).
[16] D. Rainis and D. Loss, Phys. Rev. B **90**, 235415 (2014).
[17] A. V. Moroz and C. H. W. Barnes, Phys. Rev. B **60**, 14272 (1999).
[18] D. Sánchez and L. Serra, Phys. Rev. B **74**, 153313 (2006).
[19] S. A. Gurvitz and Y. B. Levinson, Phys. Rev. B **47**, 10578 (1993).
[20] R. Winkler, *Spin-Orbit Coupling Effects in Two-Dimensional Electron and Hole Systems*, Springer Tracts in Modern Physics (Springer, Berlin, 2003).
[21] Y.-C. Xiao, R.-X. Wang, and R.-S. Yang, Superlattices Microstruct. **73**, 322 (2014).